Inorganic Chemistry

Article

pubs.acs.org/IC

Highly Flexible Molecule "Chameleon": Reversible Thermochromism and Phase Transitions in Solid Copper(II) Diiminate Cu[CF_3—C(NH)—CF═C(NH)—CF_3]$_2$

Victor N. Khrustalev,*[,†] Svetlana O. Kostenko,[†] Mikhail I. Buzin,[†] Alexander A. Korlyukov,[†] Yan V. Zubavichus,[†,‡] Michael A. Kurykin,[†] and Mikhail Yu. Antipin[†]

[†]A.N.Nesmeyanov Institute of Organoelement Compounds, Russian Academy of Sciences, 28, Vavilov Street, 119991 Moscow, Russian Federation

[‡]National Research Center "Kurchatov Institute", 1, Kurchatov Square, 123098 Moscow, Russian Federation

Supporting Information

ABSTRACT: Three thermochromic phases (α, green; β, red; γ, yellow) and six polymorphic modifications (α_1, monoclinic, $P2_1/n$, $Z = 2$; β_1, monoclinic, $P2_1/c$, $Z = 4$; β_2, triclinic, $P\bar{1}$, $Z = 4$; β_3, monoclinic, $P2_1/n$, $Z = 4$; γ_1 and γ_2, tetragonal, $P4_2/n$, $Z = 4$) have been found and structurally characterized for copper(II) diiminate Cu[CF_3—C(NH)—CF═C(NH)—CF_3]$_2$ (**1**). The α phase is stable under normal conditions, whereas the high-temperature β and γ phases are metastable at room temperature and transform slowly into the more stable α phase over several days or even weeks. X-ray diffraction study revealed that the title molecules adopt different conformations in the α, β, and γ phases, namely, staircase-like, twisted, and planar, respectively. The investigation of the α, β, and γ phases by differential scanning calorimetry showed that the three endothermic peaks in the range 283, 360, and 438 K are present on their thermograms upon heating/cooling. The two peaks at 283 and 360 K correspond to the solid−solid phase transitions, and the high-temperature peak at 438 K belongs to the melting process of **1**. The temperature and thermal effect of all the observed transitions depend on the prehistory of the crystalline sample obtained. A reversible thermochromic single-crystal-to-single-crystal $\alpha_1 \rightleftharpoons \beta_1$ phase transition occurring within a temperature interval of 353−358 K can be directly observed using a CCD video camera of the X-ray diffractometer. A series of other solid−solid $\alpha_1 \rightarrow \gamma_1$, $\beta_2 \rightarrow \gamma_1$, $\beta_3 \rightarrow \gamma_1$, and $\gamma_1 \rightleftharpoons \gamma_2$ phase transitions can be triggered in **1** by temperature. It has been suggested that, under equilibrium conditions, the $\alpha_1 \rightarrow \gamma_1$ and $\beta_2 \rightarrow \gamma_1$ phase transitions should proceed stepwise through the $\alpha_1 \rightarrow \beta_1 \rightarrow \beta_2 \rightarrow \beta_3 \rightarrow \gamma_1$ and $\beta_2 \rightarrow \beta_3 \rightarrow \gamma_1$ stages, respectively. The mechanism of the phase transitions is discussed on the basis of experimental and theoretical data.

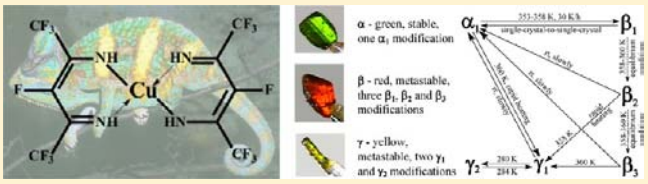

INTRODUCTION

Polymorphism is one of the most fascinating phenomena in organic and inorganic structural chemistry.[1] In some cases, different polymorphs can be obtained by tuning crystallization conditions, such as selection of an appropriate solvent, solution concentration, or crystallization temperature. However, not all possible polymorphs can be obtained in this way. Physicochemical properties of "static polymorphs" are thoroughly studied because each polymorph possesses a set of distinctive characteristics strongly affecting its functional properties. On the other hand, of particular interest are "dynamic polymorphs", i.e., polymorphic forms that undergo phase transitions on changing the environmental conditions. Such transformations from one polymorph to another can be caused by heating,[2−4] cooling,[5] or applying external pressure[6] if they are enantiotropic.[7] Over the past few years, the topic of phase transitions has become more and more popular for scientific investigation. Nevertheless, the mechanism of the phase transitions is still not fully understood.[8]

Among several kinds of single-crystal-to-single-crystal isomeric phase transformations already studied, the transformations that are attributed to a change in the coordination geometry seem to be of special interest and importance. But proper examples of this kind are quite rare.[9]

The coordination configuration of many copper(II) complexes can be readily converted from one type into another by a change in thermodynamic parameters of ambience. This structural lability clearly implies that the energy gap between different stereoisomers is rather small. Thus, many examples of solid-state thermochromism due to coordination geometry switching are known among copper(II) complexes.[10] In these complexes, minute differences in the ligands' electronic properties and steric requirements are reflected in alteration of the preferred coordination geometry when the crystal is heated or cooled. However, the systematic knowledge of factors governing the prevalence of specific coordination geometries at different temperatures is still lacking.

Herein, we report on the structural analysis of "dynamic polymorphs" of copper(II) diiminate Cu[CF_3—C(NH)—

Received: April 20, 2012
Published: September 20, 2012

 © 2012 American Chemical Society dx.doi.org/10.1021/ic300814w | *Inorg. Chem.* 2012, 51, 10590−10602

$CF{=}C(NH){-}CF_3]_2$ (**1**) demonstrating multistep reversible thermochromism to get insight into details of the phase transition mechanism. This investigation emerged as a serendipitous finding within the framework of a systematic ongoing study of thermal and sublimation behavior of transition metal β-diiminates. Remarkably, we observe no reversible thermochromism in very closely related copper(II) complexes with only one CF_3 group in the ligand of **1** replaced by a larger perfluorinated alkyl group. This fact confirms the important role of the intermolecular interligand interactions described below in the phenomenon. Recently, we confirmed the existence of two polymorphic modifications of $Cu[CF_3{-}C(NH){-}CF{=}C(NH){-}C_2F_5]_2$ and characterized them structurally, but they both were green and DSC revealed no features related to phase transitions. This will be a subject of a separate publication.

RESULTS AND DISCUSSION

Synthesis. Complex **1** was obtained by a reaction of a β-diimine $CF_3{-}C(NH){-}CF{=}C(NH_2){-}CF_3$ chloroform solution with a copper(II) diacetate water solution, according to the procedure described earlier[11] (Scheme 1).

Scheme 1

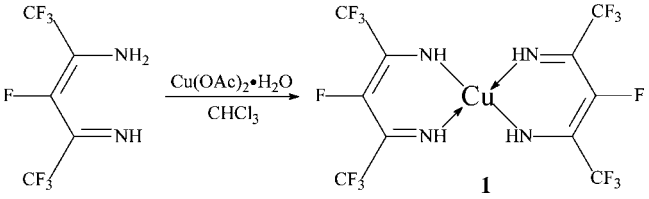

Complex **1** is a green (in the crystal at ambient conditions) and dark-brown (in a solution) substance that is quite stable both in the solid-state and in solutions at room temperature in air. It should be noted that the dark-brown solution obtained upon dissolution of the green crystals in inert solvents implies the coexistence of several conformers of **1** with small energy gaps. Compound **1** is soluble in acetone, alcohol, ether, benzene, toluene, and chloroform and insoluble in alkanes. It gave satisfactory microanalytical, IR spectroscopy, and mass-spectrometry data.

The thermogravimetric analysis (TGA) showed that compound **1** is very volatile. The mass loss takes place within a narrow temperature interval of 400−500 K as a single-stage process, and the maximum evaporation rate (minimum on the DTA curve) is achieved at 467 K (Figure 1).

Molecular and Crystal Structures. By studying the sublimation behavior of **1** we unexpectedly observed the simultaneous formation of red (β phase) and yellow (γ phase) crystals from the initial green substance (α phase) (Figure 2). These two new β and γ phases of **1** appeared to be metastable at room temperature and slowly transformed into the stable α phase over some days or even weeks.

The six polymorphic modifications of **1** were found and characterized by single-crystal X-ray diffraction study. Their structures are shown in Figure 3 along with the atomic numbering schemes. Selected bond lengths and angles are listed in Table 1. It should be noted that the α_1 modification of **1** has been recently reported;[12] however, the authors described its molecular conformation as planar, although it is better described as a staircaselike conformation as adopted in the present paper.

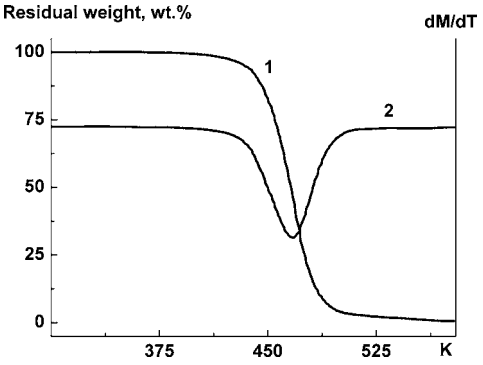

Figure 1. TGA (1) and DTA (2) curves for green crystals of **1** in an argon atmosphere upon heating at a rate of 10 K/min.

The α_1 modification of **1** thermodynamically stable at ambient conditions crystallizes in the monoclinic space group $P2_1/n$, and there is a crystallographically imposed inversion center at the Cu atom of each molecule. The Cu atom has a square-planar coordination. The diiminate ligands are also planar (rms deviation is 0.021 Å). However, the six-membered metallocycles deviate significantly from planarity and have a sofa conformation with the Cu atom out of the plane of the diiminate ligands by 0.262(1) Å. Thus, the molecule of **1** in the α_1 modification consists of three planar units adopting the staircaselike structure. The ipso-C atoms of the CF_3-substituents are slightly out of the diiminate plane by 0.164(2) and 0.133(2) Å. The CF_3-groups of each diiminate ligand are in the energetically favorable eclipsed mutual conformation. In the crystal, the molecules are packed in stacks along the *a*-axis. The molecules of different stacks are held together by weak intermolecular N−H···F hydrogen bonds (Table 2, Figure 4) as well as axial Cu···F (3.3454(7)−3.4696(8) Å) and attractive F···F interactions (Table 3, Figure 4). Notably, all four NH-protons participate in the formation of the N−H···F hydrogen bonding interactions in the crystal structure of the α_1 modification. Taking the axial Cu···F interactions into account, the Cu atom attains the [4 + 4] coordination environment. The analogous axial Cu···F interactions are often observed in solid-state structures of related fluorinated Cu(II) β-diketonate complexes.[13]

In the molecular structures of the β_1, β_2, and β_3 modifications of **1**, contrary to the α_1 modification, the six-membered metallocycles are virtually planar (rms deviations are 0.015/0.040, 0.018/0.016, and 0.009/0.015 for two crystallographically independent molecules and 0.010/0.011 Å, respectively) and twisted relative to each other by 18.0(1)°, 16.2(2)°, and 28.2(2)° (for the two crystallographically independent molecules) and 23.2(1)°, respectively (Figure 3). As a result, the Cu atom acquires a distorted tetrahedral geometry. Similar to the α_1 modification, the ipso-C atoms of the CF_3-substituents in the β_1, β_2, and β_3 modifications are slightly out of the planes defined by the six-membered metallocycle by 0.013(6)−0.080(6) (except for the C10 carbon atom), 0.015(7)−0.180(7), and 0.051(7)−0.135(7) (for the two crystallographically independent molecules) and 0.038(5)−0.073(4) Å, respectively. The CF_3-groups of each diiminate ligand are in the eclipsed (for the β_1 modification), slightly staggered and eclipsed (for the two crystallographically

dx.doi.org/10.1021/ic300814w | Inorg. Chem. 2012, 51, 10590−10602

Figure 2. Shape and color for α (green, top), β (red, middle), and γ (yellow, bottom) phases of **1**.

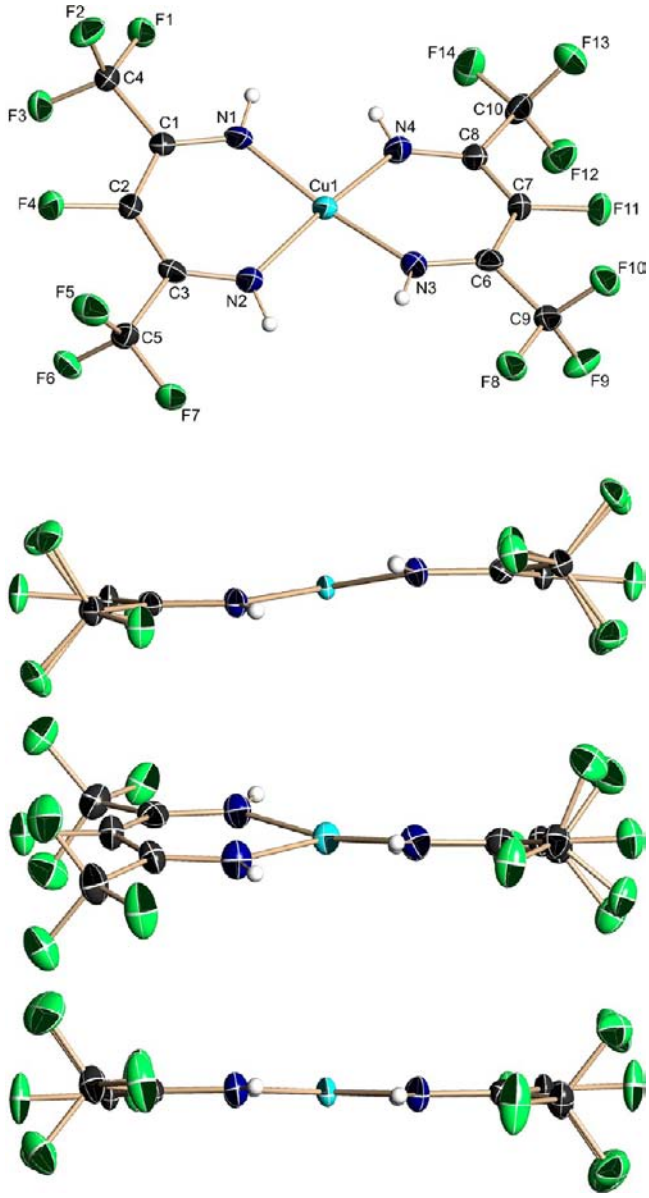

Figure 3. Molecular structures of the α (staircaselike), β (twisted), and γ (planar) phases of **1** (50% ellipsoids). The atomic numbering scheme corresponds to the β phase. In the α and γ phases, only one of the two diiminate ligands is symmetrically unique.

independent molecules in the β_2 modification), and slightly staggered (for the β_3 modification) mutual conformations.

The crystal structures of the β_1, β_2, and β_3 modifications significantly differ by symmetry from each other. The β_1 modification crystallizes in the monoclinic space group $P2_1/c$, Z = 4, with one molecule per asymmetric unit. The β_2 modification crystallizes in the triclinic space group $P\bar{1}$, Z = 4, with two crystallographically independent molecules per asymmetric unit. The β_3 modification crystallizes in the monoclinic space group $P2_1/n$, Z = 4, with one molecule per asymmetric unit. The crystal packings of the β_1, β_2, and β_3 modifications can be described as molecular stackings along the c (β_1 modification), a (β_2 modification), and a (β_3 modification) axes. The most striking difference between these crystal structures is manifested in the pattern of weak intermolecular interactions (Tables 2 and 3). In particular, in the crystal structure of the β_1 modification, no N−H···F hydrogen bond is present. The Cu atom forms only one weak additional Cu···F interaction (3.374(3) Å) forming the [4 + 1] coordination environment. Furthermore, there are only two attractive intermolecular F···F interactions. The intermolecular Cu···F and F···F interactions link the molecules of different stacks into zigzaglike chains along the b axis (Figure 5). In the crystal structure of the β_2 modification, only three NH-protons of one crystallographically independent molecule form weak

dx.doi.org/10.1021/ic300814w | *Inorg. Chem.* 2012, 51, 10590−10602

Table 1. Selected Bond Lengths (Å) and Angles (deg) for the α_1, β_1, β_2, β_3, γ_1, and γ_2 Modifications of 1

modification	α_1[a]	β_1	β_2[b]	β_3	γ_1[a]	γ_2[a]
Cu1−N1	1.960(1)	1.933(2)	1.940(4); 1.934(4)	1.944(2)	1.946(2)	1.9500(15)
Cu1−N2	1.950(1)	1.935(2)	1.943(4); 1.942(4)	1.937(2)	1.945(2)	1.9511(15)
Cu1−N3		1.933(3)	1.953(4); 1.942(4)	1.935(2)		
Cu1−N4		1.933(2)	1.944(4); 1.944(4)	1.935(2)		
N1−C1	1.309(1)	1.293(3)	1.316(6); 1.317(6)	1.303(3)	1.306(3)	1.308(2)
N2−C3	1.312(1)	1.308(4)	1.314(6); 1.313(6)	1.306(3)	1.305(3)	1.313(2)
N3−C6		1.298(3)	1.306(6); 1.305(5)	1.295(3)		
N4−C8		1.305(3)	1.309(6); 1.308(5)	1.306(3)		
C1−C2	1.390(1)	1.380(4)	1.375(6); 1.385(6)	1.382(4)	1.371(4)	1.389(2)
C2−C3	1.390(1)	1.368(5)	1.389(6): 1.386(6)	1.380(3)	1.375(4)	1.384(2)
C6−C7		1.381(4)	1.390(6); 1.388(6)	1.375(4)		
C7−C8		1.367(4)	1.377(6); 1.387(6)	1.383(4)		
N1−Cu1−N2	89.53(4)	89.8(1)	89.9(2); 90.5(2)	89.9(1)	89.16(10)	89.69(6)
N1−Cu1−N3		167.0(1)	169.2(2); 161.7(2)	164.8(1)		
N1−Cu1−N4		91.0(1)	91.1(2); 93.1(2)	92.7(1)		
N2−Cu1−N3		92.2(1)	91.4(2); 92.5(2)	92.1(1)		
N2−Cu1−N4		168.3(1)	167.7(2); 159.5(2)	163.3(1)		
N3−Cu1−N4		89.5(1)	89.9(2); 90.4(2)	89.8(1)		
C1−N1−Cu1	128.14(8)	129.1(2)	129.1(3); 128.7(3)	128.6(2)	129.0(2)	128.92(13)
C3−N2−Cu1	128.38(8)	128.6(2)	128.2(3); 128.0(3)	129.0(2)	129.1(2)	128.53(13)
C6−N3−Cu1		129.1(2)	128.3(3); 128.5(3)	129.2(2)		
C8−N4−Cu1		128.3(2)	128.7(3); 128.7(3)	128.5(2)		
N1−C1−C2	123.69(10)	123.0(3)	123.4(4); 123.5(4)	123.7(2)	123.6(2)	123.6(2)
N2−C3−C2	123.65(10)	123.2(3)	124.0(4); 124.1(4)	123.3(2)	123.5(2)	123.9(2)
N3−C6−C7		123.2(3)	123.8(4); 123.1(4)	123.6(2)		
N4−C8−C7		124.1(3)	123.8(4); 122.7(4)	123.7(2)		
C1−C2−C3	124.91(10)	126.1(3)	125.2(4); 125.1(4)	125.6(2)	125.5(2)	125.0(2)
C6−C7−C8		125.0(3)	125.1(4); 126.4(4)	125.2(2)		

[a]The molecules occupy a special position on the inversion center. [b]For the two independent molecules.

Table 2. Intermolecular N−H···F Hydrogen Bonds (Å and deg) for the α_1, β_1, β_2, β_3, γ_1, and γ_2 Modifications of 1

D[a]−H···A[a]	d(D−H)	d(H···A)	d(D···A)	∠(D−H···A)
Modification α_1				
N1−H1···F4[b]	0.88	2.48	3.256(1)	147
N2−H2···F4[c]	0.88	2.54	3.401(1)	167
Modification β_1				
Modification β_2				
N5−H5···F23[d]	0.88	2.33	3.176(5)	161
N7−H7···F11	0.88	2.46	3.324(4)	166
N8−H8···F19[e]	0.88	2.41	3.261(5)	161
Modification β_3				
N3−H3···F2[f]	0.86	2.47	3.211(3)	145
Modification γ_1				
N1−H1···F2[g]	0.86	2.56	3.413(3)	173
N2−H2···F2[h]	0.86	2.57	3.418(3)	170
Modification γ_2				
N1−H1···F5[i]	0.88	2.50	3.362(2)	167
N2−H2···F5[j]	0.88	2.45	3.327(2)	173

[a]D, protonodonor; A, protonoacceptor. [b]Symmetry transformations used to generate equivalent atoms: [$x - {}^1/_2, -y + {}^3/_2, z - {}^1/_2$]. [c][$-x + {}^1/_2, y + {}^1/_2, -z + {}^3/_2$]. [d][$-x, -y + 2, -z + 1$]. [e][$-x + 1, -y + 2, -z + 1$]. [f][$-x + 2, -y, -z + 1$]. [g][$y - {}^1/_2, -x + 1, z - {}^1/_2$]. [h][$-y + {}^1/_2, x, -z + {}^1/_2$]. [i][$y, -x + {}^1/_2, -z + {}^1/_2$]. [j][$-y + 1, x + {}^1/_2, z - {}^1/_2$].

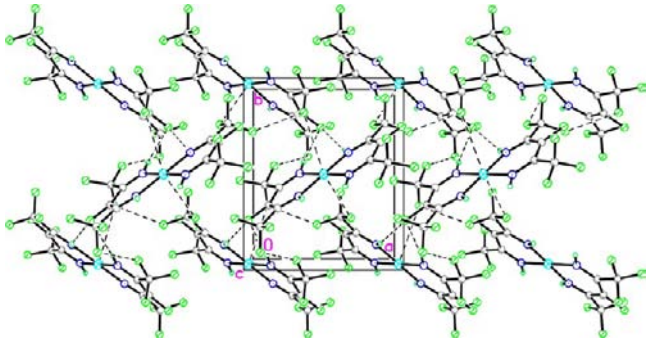

Figure 4. Crystal packing of molecules of the α_1 modification of **1** along the *c*-axis. Dashed lines indicate the intermolecular N−H···F, Cu···F, and F···F interactions.

N−H···F hydrogen bonds, while the second independent molecule does not form similar H-bonds. The Cu1 atom of the first molecule forms only one weak additional Cu···F interaction (3.291(3) Å) composing the [4 + 1] coordination geometry, whereas the Cu2 atom of the second molecule forms two additional weak Cu···F interactions (3.080(3) and 3.198(3) Å) with the [4 + 2] coordination configuration. The molecules within the stacks are bound by the N−H···F hydrogen bonds, axial Cu···F, and attractive F···F interactions, whereas the N−H···F hydrogen bonds and attractive F···F interactions link molecules between neighboring stacks (Figure 6). In the crystal structure of the β_3 modification, only one independent intermolecular weak N−H···F hydrogen bond is present. The Cu atom forms two additional weak Cu···F interactions (3.318(2) and 3.516(2) Å, one of them is too weak and might be considered as essentially nonbonding) adopting the [4 + 2] coordination geometry. The molecules within the stacks are bound by the N−H···F hydrogen bonds and axial Cu···F

dx.doi.org/10.1021/ic300814w | Inorg. Chem. 2012, 51, 10590−10602

Table 3. Intermolecular Cu···F and F···F Short Contacts (Å) for the α_1, β_1, β_2, β_3, γ_1, and γ_2 Modifications of 1

Modification α_1			
Cu1···F3[a]	3.3454(7)	F1···F7[e]	2.774(1)
Cu1···F3[b]	3.3454(7)	F7···F1[c]	2.774(1)
Cu1···F6[c]	3.4696(8)	F2···F6[f]	2.877(1)
Cu1···F6[d]	3.4696(8)	F6···F2[b]	2.877(1)
Modification β_1			
Cu1···F5[g]	3.374(3)	F3···F6[h]	2.776(4)
		F6···F3[g]	2.776(4)
Modification β_2			
Cu1···F2[i]	3.291(3)	F1···F9[l]	2.870(5)
Cu2···F15[j]	3.080(3)	F9···F1[l]	2.870(5)
Cu2···F27[k]	3.198(3)	F1···F18[m]	2.858(4)
		F18···F1[n]	2.858(4)
		F2···F26[o]	2.729(4)
		F26···F2[o]	2.729(4)
		F3···F28[p]	2.730(4)
		F28···F3[q]	2.730(4)
		F6···F15[r]	2.857(5)
		F15···F6[r]	2.857(5)
		F7···F24[l]	2.878(4)
		F24···F7[l]	2.878(4)
		F8···F27[s]	2.832(4)
		F27···F8[t]	2.832(4)
		F11···F22	2.816(5)
		F22···F11	2.816(5)
		F16···F23[k]	2.843(5)
		F23···F16[k]	2.843(5)
Modification β_3			
Cu1···F5[u]	3.516(2)	F1···F4[w]	2.857(3)
Cu1···F8[v]	3.318(2)	F4···F1[x]	2.857(3)
		F6···F8[y]	2.892(3)
		F8···F6[e]	2.892(3)
		F7···F9[z]	2.768(3)
		F9···F7[aa]	2.768(3)
		F9···F13[bb]	2.878(4)
		F13···F9[a]	2.878(4)
Modification γ_1			
Cu1···F4[m]	3.580(2)	F4···F5[dd]	2.894(3)
Cu1···F4[cc]	3.580(2)	F5···F4[ee]	2.894(3)
Modification γ_2			
Cu1···F4[m]	3.454(1)	F1···F4[gg]	2.789(2)
Cu1···F4[ff]	3.454(1)	F4···F1[hh]	2.789(2)

[a]Symmetry transformations used to generate equivalent atoms: [−x + 1/2, y + 1/2, −z + 1/2]. [b][x − 1/2, −y + 3/2, z + 1/2]. [c][−x + 1/2, y + 1/2, −z + 3/2]. [d][x − 1/2, −y + 3/2, z − 1/2]. [e][−x + 1/2, y− 1/2, −z + 3/2]. [f][x + 1/2, −y + 3/2, z − 1/2]. [g][−x + 2, y + 1/2, −z + 1/2]. [h][−x + 2, y − 1/2, −z + 1/2]. [i][−x + 2, −y + 1, −z]. [j][−x + 1, −y + 2, −z + 1]. [k][−x, −y + 2, −z + 1]. [l][−x + 1, −y + 1, −z]. [m][x, y, z − 1]. [n][x, y, z + 1]. [o][−x + 1, −y + 2, −z]. [p][x + 2, y − 1, z − 1]. [q][x − 1, y + 2, z + 2]. [r][−x + 2, −y + 1, −z + 1]. [s][x + 1, y − 1, z]. [t][x − 1, y + 1, z]. [u][−x + 2, −y, −z + 1]. [v][−x + 1, −y, −z + 1]. [w][x − 1/2, −y + 1/2, z − 1/2]. [x][x + 1/2, −y + 1/2, z + 1/2]. [y][−x + 3/2, y + 1/2, −z + 3/2]. [z][x + 1/2, −y − 1/2, z + 1/2]. [aa][x − 1/2, −y − 1/2, z − 1/2]. [bb][−x + 1/2, y − 1/2, −z + 1/2]. [cc][−x + 1, −y + 1, −z + 2]. [dd][y, −x + 3/2, −z + 5/2]. [ee][−y + 3/2, x, −z + 5/2]. [ff][−x + 1, −y + 1, −z + 1]. [gg][y, −x + 1/2, −z + 3/2]. [hh][−y + 1/2, x, −z + 3/2].

interactions, whereas only attractive F···F interactions link molecules between the stacks (Figure 7).

The γ_1 and γ_2 modifications crystallize in the tetragonal space group $P4_2/n$, and there is a crystallographically imposed

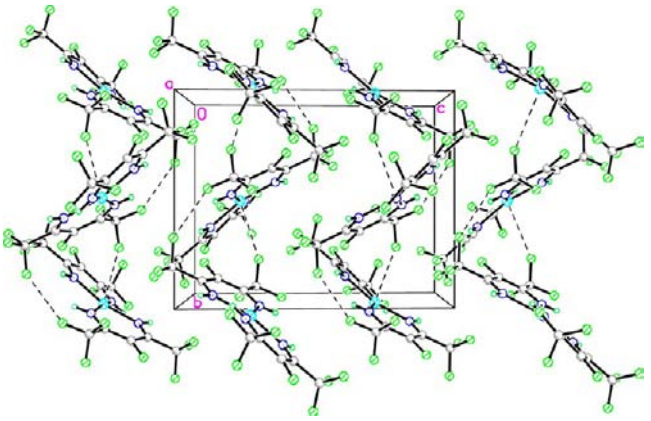

Figure 5. Crystal packing of molecules of the β_1 modification of **1** along the *a*-axis. Dashed lines indicate the intermolecular Cu···F and F···F interactions.

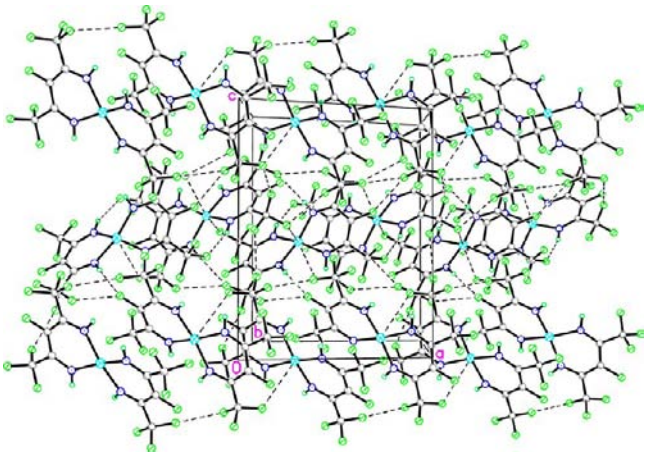

Figure 6. Crystal packing of molecules of the β_2 modification of **1** along the *c*-axis. Dashed lines indicate the intermolecular N−H···F, Cu···F, and F···F interactions.

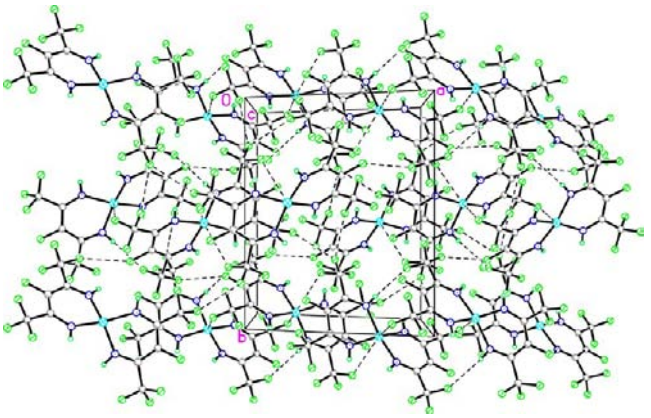

Figure 7. Crystal packing of molecules of the β_3 modification of **1** along the *c*-axis. Dashed lines indicate the intermolecular N−H···F, Cu···F, and F...F interactions.

inversion center at the Cu atom of each molecule. In contrast to the α_1, β_1, β_2, and β_3 modifications, the molecular structures of the γ_1 and γ_2 modifications are almost planar (rms deviations are 0.017 and 0.026 Å, respectively, Figure 3). The ipso-C atoms of the CF_3-substituents and fluorine F4 atom are only slightly out of these planes by 0.076(5), 0.081(5), 0.061(4) and

dx.doi.org/10.1021/ic300814w | Inorg. Chem. 2012, 51, 10590−10602

0.113(3), 0.120(3), 0.070(2) Å, respectively. The CF_3-groups of each diiminate ligand are in the energetically favorable eclipsed mutual conformation. The crystal structures of these modifications are also very similar (Figures 8 and 9). As for the

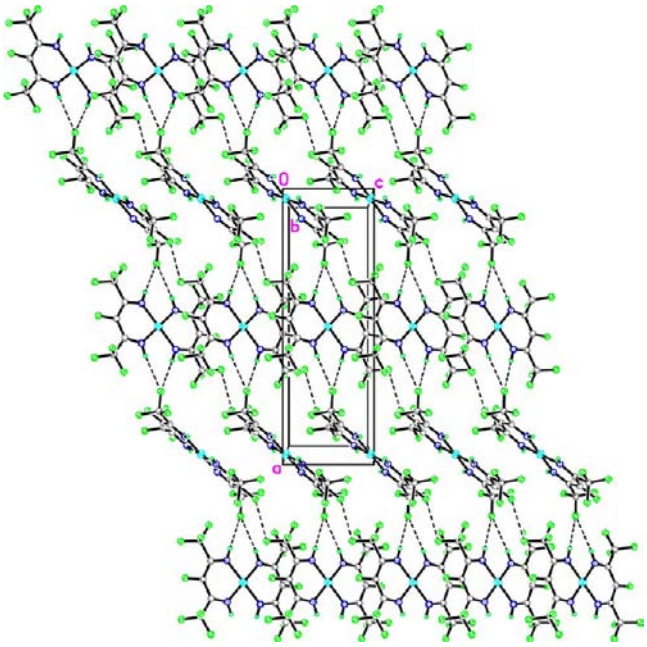

Figure 8. Crystal packing of molecules of the γ_1 modification of **1** along the *b*-axis. Dashed lines indicate the intermolecular N−H···F and F···F interactions.

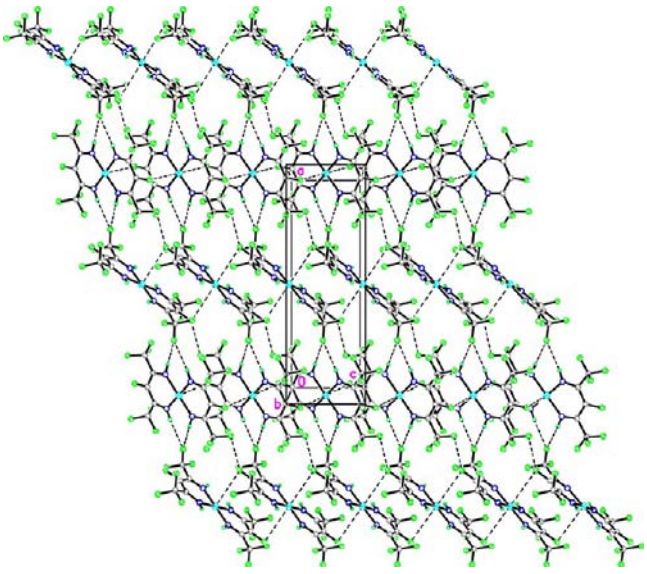

Figure 9. Crystal packing of molecules of the γ_2 modification of **1** along the *b*-axis. Dashed lines indicate the intermolecular N−H···F, Cu···F, and F···F interactions.

α_1 modification, all four NH-protons are involved in weak intermolecular N−H···F hydrogen bonding interactions (Table 2). The molecules are linked into a three-dimensional framework by two intermolecular attractive F···F interactions (Table 3). Nevertheless, the crystal structures of the γ_1 and γ_2 modifications differ from each other by the coordination environment of the copper(II) atoms. So, the Cu atom in the γ_2 modification forms two weak axial Cu···F interactions (3.454(1) Å) composing a strongly distorted octahedral [4 + 2] coordination environment, whereas the axial Cu···F distances in the γ_1 modification (3.580(2) Å) are very long and rather correspond to nonbonding interactions (Table 3). Moreover, all the N−H···F and F···F intermolecular interactions in the γ_1 modification are significantly weakened as compared to those in the γ_2 modification.

More insight to the explanation of the stability of the modifications obtained came from the topological analysis of electron density distribution function in terms of Bader's "atoms in molecules theory".[14] The application of this theoretical approach allowed us to study in detail the peculiarities of the intermolecular interactions in their crystal structures. The energy of intermolecular interactions found was estimated using the empirical correlation formula proposed by Espinosa, Mollins, and Lecomte.[15] The total energy of all intermolecular interactions is the sublimation energy at 0 K (E_{subl}) without the contribution due to molecular relaxation upon transition from the crystalline to gas phase. As can be seen from Table 4, the quantum-chemical calculations show that the stability of the six modifications of **1** decreases in the series $\alpha_1 > \beta_2 > \gamma_1(\gamma_2) > \beta_3 > \beta_1$.

Table 4. Quantum-Chemical Calculations of Crystal Structures for the Six Modifications of 1

param	α_1	β_1	β_2	β_3	γ_1/γ_2
ΔE, kcal/mol	0	12.76	4.80	10.57	4.84
E_{subl}, kcal/mol	38.5	20.3	33.7	24.5	34.1
V, Å^3	741.32	1651.67	1545.43	1632.62	1560.93
Cu1−N1, Å	1.965	1.951	1.954	1.954	1.961
Cu1−N2, Å	1.955	1.955	1.956	1.959	1.959
Cu1−N3, Å		1.963	1.962	1.948	
Cu1−N4, Å		1.951	1.958	1.955	
Cu2−N5, Å			1.949		
Cu2−N6, Å			1.952		
Cu2−N7, Å			1.953		
Cu2−N8, Å			1.955		

It is important to note that the crystallographic densities of the modifications studied at 100 K decrease in the following series α_1 (2.278 g/cm^3) > β_2 (2.186 g/cm^3) > γ_2 (2.158 g/cm^3), while density of the γ_1 modification at room temperature (2.091 g/cm^3) exceeds that of the β_3 modification (2.065 g/cm^3). Consequently, the Kitaigorodskii's maximum density rule ("the denser, the more stable") is met in this case.[16]

Molecular Structure of 1 in Solutions. As it has been mentioned above, dissolution of **1** in benzene affords a dark-brown solution irrespective of the specific colored polymorph taken for the solution preparation. Tentatively, this means that different conformers of **1** similar to those found in crystal structures of the 6 polymorphic modifications coexist in a solution in energetics-driven proportions. In order to verify the assumption we performed a comparative X-ray absorption spectroscopy study of **1** as a solid and as a solution. As representative examples of crystalline polymorphs we used green α_1 and red β_3 modifications, which can be relatively easily isolated as strictly single-phase polycrystalline powders in quantities sufficient for the characterization via sublimation or heating. The phase purity of the powder samples was carefully checked and confirmed by powder X-ray diffraction (see Supporting Information).

dx.doi.org/10.1021/ic300814w | *Inorg. Chem.* 2012, 51, 10590−10602

The experimental Cu K-edge XANES spectra for the two solids and their derived saturated benzene solutions are shown in Figure 10. Three major features are clearly distinguishable in

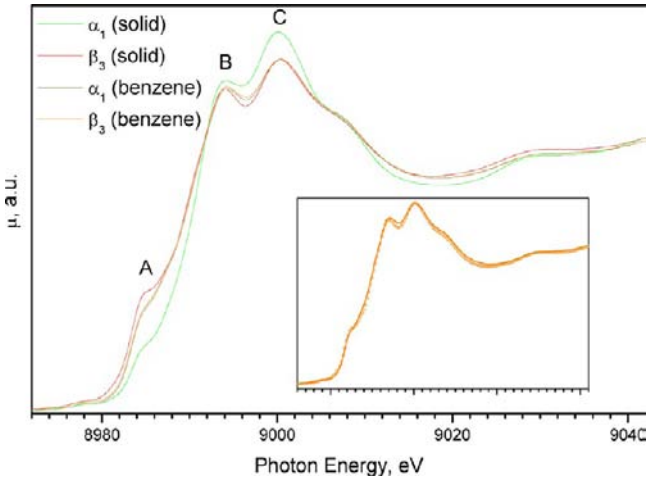

Figure 10. Cu K-edge XANES spectra of strictly single-phase green α_1 and red β_3 polymorphs of **1** as polycrystalline powders and their derived benzene solutions. The inset shows a simulation of the experimental spectrum of β_3 benzene solution (—) by a linear combination of spectra of the two solids (○).

the experimental spectra denoted as A, B, and C. Importantly, the first feature A observed at ca. 8985 eV is traditionally assigned to the dipole-allowed $1s \rightarrow 4p_z$ electronic transition, which is very sensitive to the coordination geometry.[17] In particular, for tetracoordinated Cu(II) complexes, the intensity of A hits the maximum for square-planar configuration and gets nearly totally suppressed for the ideal tetrahedral coordination. In this respect, the strongly attenuated intensity of A in the case of the solid red polymorph is fully consistent with the structural results discussed above. Indeed, the molecular geometry of copper diiminate **1** is characterized by the maximum deviation from planarity in the case of the α_1 modification.

The experimental XANES spectra of the two benzene solutions (i) are very similar to each other, (ii) lie in-between the experimental spectra for the two solids over entire spectral range, and (iii) are closer to the red sample rather than green one. This means that the local coordination geometry of the Cu atom in benzene solutions of **1** differs from any single conformation found in the six polymorphic modifications (see below) and should rather be represented as their superposition due to the dynamic equilibrium. Here, we should note that the intensity of feature A for the yellow polymorph is expected to be even larger than for the red one (due to difficulties in the isolation and instability of the yellow polymorph, no experimental study has been performed so far), and thus, the above statement is valid even if we take the yellow polymorphic modification of **1** into consideration as well.

The experimental spectra for the two benzene solutions derived from the green and red powders were simulated using linear combinations of the respective spectra of solids. The best-fit fractions of the components are as follows: solution from green solid = 0.21(solid green) + 0.79(solid red); solution from red solid = 0.17(solid green) + 0.83(solid red) with an estimated accuracy of the coefficients of ±0.05. Thus, both solutions are dominated by red conformers, and although the best-fit fractions of the components are nominally identical within the error bars, the minute difference observed can be due to the fact that the solutions were not fully equilibrated after preparation.

The UV absorption spectra of hexane solutions of the green and red phases of **1** are fully equivalent. The spectra contain a strong band in the region 250−450 nm with the main maximum at 364 nm and weaker submaxima at 316 and 390 nm. Only the right-hand wing of the absorption band extending to the visible range can be responsible for the apparent color of the solution. Surprisingly, solid-state UV−vis spectra of red and green phases look very similar to the solution spectra except for the emergence of rather weak bands at ca. 580 and 730 nm. Although no strict assignment of these bands is currently available due to problems with the preparation of single-phase samples, probably they are related to the color changes.

Study of Phase Transitions. The differential scanning calorimetry (DSC) is the method-of-choice to detect temperature-triggered phase transitions by observing heat anomalies during heating or cooling. For crystals of the α phase of **1**, DSC reveals two endothermic peaks at 360 and 439 K upon heating at a ramp rate of 10 K/min (Figure 11, top; Table 5). Remarkably, the peak at 360 K was irreversible since it appeared neither upon cooling nor repeated heating of the same sample. Instead, two other exothermic peaks at 398 and 280 K and the two endothermic peaks at 284 and 428 K were identified in DSC curves, respectively (Table 5). Evidently, the peaks at 360 and 280/284 K are due to solid−solid phase transitions, whereas the peaks at 439(428)/398 K correspond to melting/crystallization of **1**. The latter high-temperature transformations of **1** possess a considerable temperature hysteresis, which can be explained by different quality of crystals formed in the sublimation process and rapid crystallization from a melt.

In order to elucidate the thermal behavior of **1** more precisely we have also performed similar DSC measurements with crystals of the β-red and γ-yellow phases obtained by the sublimation of the α-green phase (Figure 11, middle and bottom; Table 5). Surprisingly, we found that the DSC curves for the β-red phase are very similar to those of the α phase both upon heating and cooling, whereas the γ phase demonstrated only peaks observed for the α and β phases upon cooling (after the first heating) and repeated heating. These observations can be rationalized assuming that both the α-green and β-red crystals irreversibly transform into the γ-yellow phase at 360 K, which then undergoes only one low-temperature reversible phase transition. Moreover, a DSC study of a yellow crystal formed by heating a green crystal performed one month later demonstrated that, indeed, it had transformed back into the green phase (Figure 11, top, curve 4), even though thermal effects of the phase transitions decreased significantly (Table 5). The sharp shape of the peaks is indicative that the respective phase transitions are of the first order.

The solid−solid phase transitions of **1** were further investigated by variable-temperature single-crystal X-ray diffraction over a temperature interval 100−400 K. The thermodynamically stable α-green phase of **1** contains the only α_1-modification, which is monoclinic with the space group $P2_1/n$ and $Z = 2$ (the molecule in the crystal occupies a special position on an inversion center). This phase changes neither color nor unit-cell parameters (except for uniform temperature contraction) upon cooling down to 100 K. However, it turns red upon heating above 330 K and transforms into the β_1-red modification within a temperature interval 353−358 K, with the

dx.doi.org/10.1021/ic300814w | Inorg. Chem. 2012, 51, 10590−10602

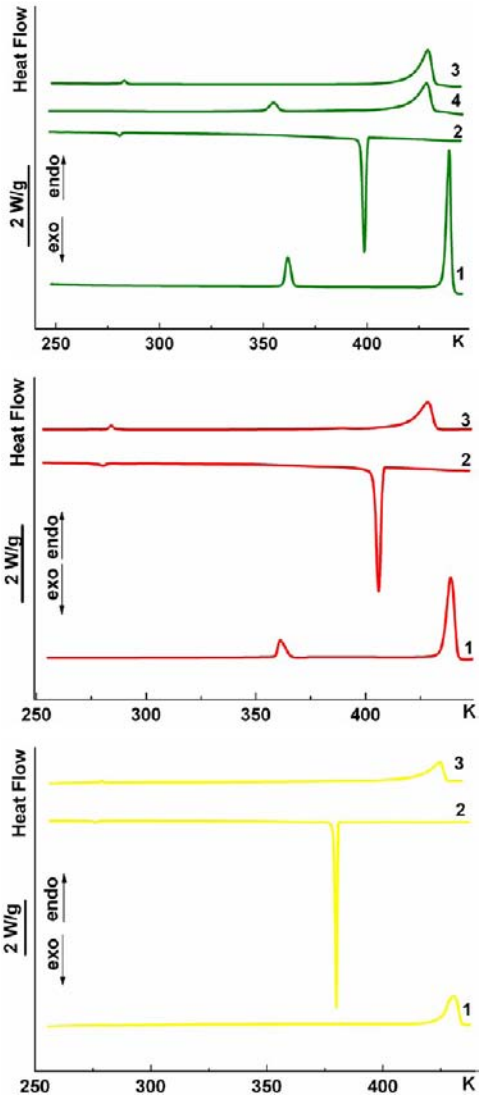

Figure 11. DSC curves for the α (green, top), β (red, middle) and γ (yellow, bottom) phases of **1** at first (1), second (3) heating and cooling (2) upon heating/cooling at a rate of ±10 K/min. Curve 4 corresponds to the green phase formed spontaneously upon storage of a crystallized melt of **1** at room temperature for a month.

monoclinic space group $P2_1/c$ and $Z = 4$ (the molecule in the crystal occupies a general position). The single-crystal-to-single-crystal phase transition $\alpha_1 \rightleftharpoons \beta_1$ can be directly observed using a CCD video camera installed on the X-ray diffractometer. It is important to point out that the single crystals of the α_1 modification are cracked upon heating at a ramp rate exceeding 30 K/h, but remain intact at a slower heating rate. Moreover, this phase transition is reversible and can be repeated several times without significant degradation of the crystal quality. All our attempts to heat single crystals of the β_1 modification to above 358 K, even at a ramp rate as low as 1 K/h, caused them to crumble into microcrystalline powder. The fact that the solid−solid phase transition $\alpha_1 \rightleftharpoons \beta_1$ eludes detection by DSC can be explained by the nonequilibrium character of the process upon rapid heating.

Furthermore, the X-ray diffraction study of red crystals obtained by sublimation of the green phase revealed two other metastable modifications of **1**, viz., β_2 (triclinic space group $P\bar{1}$, $Z = 4$) and β_3 (monoclinic space group $P2_1/n$, $Z = 4$). It is the sublimation temperature that governs which of the two modifications is formed: the β_3 modification is formed at a higher sublimation temperature, whereas the β_2 is preferably formed at a lower sublimation temperature. Interestingly, single crystals of the β_2 modification remain unbroken and unchanged upon cooling down to 100 K, but crack upon heating above 360 K, whereas single crystals of the β_3 modification crack both upon heating above 360 K and cooling down to 100 K. Therefore, the β-red phase of **1** is actually composed of three polymorphic modifications β_1, β_2, and β_3. They are numbered according to their molecular structures (see next paragraph), since the β_2 modification is intermediate between β_1 and β_3 in terms of ligand twist angles within the molecules. Moreover, obviously, the endothermic DSC peaks at 360 K correspond to the apparent total thermal effects of the $\alpha_1 \rightarrow \gamma_1$, $\beta_2 \rightarrow \gamma_1$, and $\beta_3 \rightarrow \gamma_1$ phase transitions due to the nonequilibrium character of the process upon rapid heating. Nevertheless, we can anticipate $\beta_1 \rightarrow \beta_2 \rightarrow \beta_3$ phase transitions within the $\alpha_1 \rightarrow \gamma_1$ and $\beta_2 \rightarrow \gamma_1$ (the $\beta_2 \rightarrow \beta_3$ phase transition only) phase transitions upon heating, which should be energetically feasible (see the last paragraph). In our opinion, the situation can be clarified in further investigations applying the adiabatic calorimetry under experimental conditions maximally close to the equilibrium ones.

Finally, the metastable γ-yellow phase changes neither color nor crystal system over a temperature interval of 100−400 K. It is tetragonal with the $P4_2/n$ space group and $Z = 4$ (the molecule in the crystal occupies a special position on an inversion center). The low-energy low-temperature reversible phase transition $\gamma_1 \rightleftharpoons \gamma_2$ observed by DSC is explained by the significant weakening of additional intermolecular interactions (or even complete absence of some of them) in the γ_1 phase compared to the γ_2 phase (see below). It should be noticed that the thermal effect of the $\gamma_1 \rightleftharpoons \gamma_2$ phase transition calculated from the DSC measurements depends from sample prehistory and takes up a minimal value for the sample obtained by sublimation (Table 5).

Table 5. Thermal Effects for Different Modifications of 1 Observed by DSC Method

	first heating				cooling				second heating			
modification	$T_{c\text{-}c}$, K	$\Delta H_{c\text{-}c}$, kJ/mol	T_m, K	ΔH_m, kJ/mol	T_{cryst}, K	ΔH_{cryst}, kJ/mol	$T_{c\text{-}c}$, K	$\Delta H_{c\text{-}c}$, kJ/mol	$T_{c\text{-}c}$, K	$\Delta H_{c\text{-}c}$, kJ/mol	T_m, K	ΔH_m, kJ/mol
α_1-green	360	5.54	439	23.67	401	19.35	281	0.57	283	0.57	429	19.31
α_1-green[a]	354	2.64	429	16.05								
β_2-red	358	5.34	438	25.38	408	19.92	281	0.33	283	0.33	432	20.04
β_3-red	360	5.54	438	23.83	408	18.90	280	0.67	284	0.67	428	19.06
γ_1-yellow	283	0.23	430.3	17.37	280	16.54	381	0.58	284	0.58	424	16.54

[a]The yellow phase prepared from the initial green phase by heating turned back into the green phase spontaneously upon storage for a month.

dx.doi.org/10.1021/ic300814w | Inorg. Chem. 2012, 51, 10590−10602

Thus, all phase transitions found for **1** are given in Scheme 2. Although topochemical reactions in the solid state are well documented,[18,19] single-crystal-to-single-crystal phase transitions are rare since they commonly give rise to a substantial degradation of the crystal quality and increased mosaicity, which are manifested in very weak diffraction signal at high scattering angles. Moreover, reversible phase transitions between distinctive molecular structures are exceptionally rare,[20] perhaps due to the fact that cooperative molecular rearrangements in such systems are rarely accompanied by the retention of the overall structure's integrity. It is worth stressing here that temperature induced phase transitions should be always taken into account when examining solid state properties of bulk crystalline materials and considering their structure–property relationships.

Scheme 2

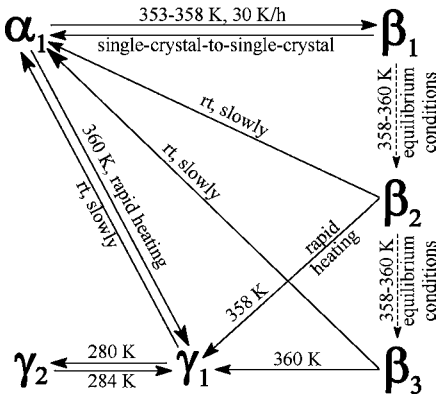

Thermochromism and Phase Transition Mechanism. Thermochromism is a well-known phenomenon in coordination chemistry and is usually ascribed to temperature-driven changes in the coordination geometry of chromophore groups. Thermochromic behavior of several copper(II) complexes has been studied in some detail previously.[21−25] The authors

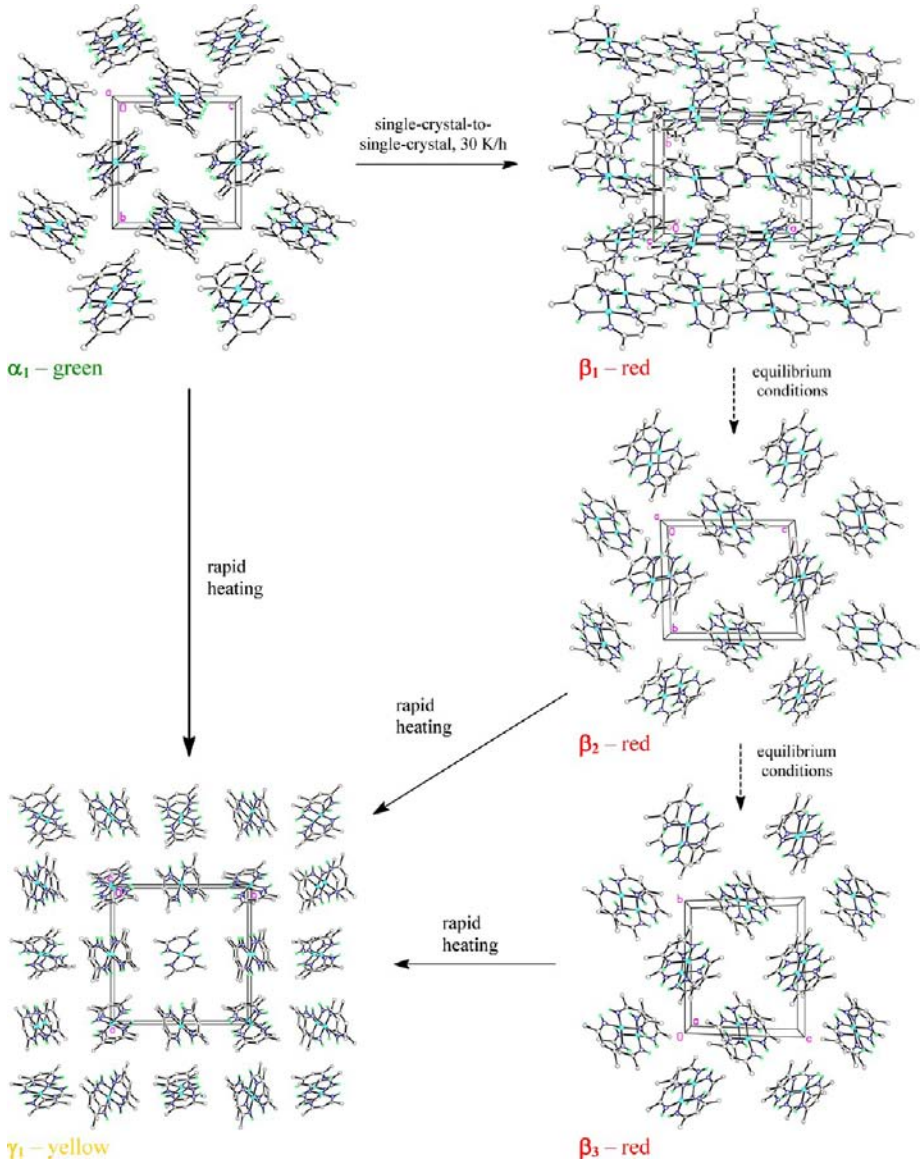

Figure 12. Changes in molecular packing of the five modifications of **1** upon heating. The dashed arrows indicate possible equilibrium solid–solid $\beta_1 \rightarrow \beta_2 \rightarrow \beta_3$ phase transitions. The fluorine atoms are omitted for clarity.

dx.doi.org/10.1021/ic300814w | *Inorg. Chem.* 2012, 51, 10590−10602

pointed out either temperature-dependent distortion of the copper(II) coordination configuration (from square-planar to tetragonally distorted octahedral with weakened axial interactions)[21,22] or a change in the in-plane ligand field strength[25] as probable mechanisms of the thermochromism.

In the case of **1**, the thermochromism observed experimentally can be also explained by geometrical reasons. However, the principal difference in our case is that the first-shell copper(II) coordination environment undergoes a temperature-dependent distortion (from square-planar in the α phase to distorted tetrahedral in the β phase, and then back to square-planar in the γ phase) rather than second-shell coordination. Indeed, additional axial Cu···F interactions are very weak and, in particular, cause no thermochromic changes in the γ_2 modification relative to the γ_1 modification). The difference in color between the α and γ phases of **1** is related to a decrease in the degree of involvement of Cu orbitals in bonding with the in-plane ligands for the α phase due to the staircase-like molecular structure, as compared to nearly planar molecular structure of the γ phase. A slight elongation of the Cu−N bonds in the α phase (Table 1) is fully consistent with the statement.

Remarkably, Riley et al.[26] have reported on piperazinium tetrachlorocuprate(II) complex $(pipzH_2)_2[CuCl_4]\cdot Cl_2\cdot 3H_2O$, in which, similarly to **1**, a solid-state thermochromic transition from green to yellow color was attributed to a D_{4h} (square planar) → D_{2d} (flattened tetrahedron) distortion of the $CuCl_4^{2-}$ ion. Notably, the color of a polymorphic modification is determined not only by the copper(II) coordination geometry but also by other factors, such as in-plane bonding strength within ligands and additional intermolecular interactions accompanying changes in the copper d-orbital energies.

Although additional weak intermolecular interactions (including N−H···F hydrogen bonds, axial Cu···F and attractive F···F interactions) do not induce thermochromic changes in solid **1** directly, they govern the relative stabilities of the six polymorphic modifications of **1**. It is important to note that the α_1, β_1, β_2, β_3, γ_1, and γ_2 modifications are characterized by 12, 3, 12, 11, 6, and 8 additional intermolecular interactions per molecule, respectively, which correlates well with their stability. Moreover, the weak N−H···F hydrogen bonding interactions appear in the IR spectrum of solid **1** (stable α green phase) as a weak broadened satellite at 3366 cm^{-1} slightly red-shifted from the main narrow intense band. Apparently, it is the formation of weak intermolecular interactions that act as the driving force of the solid−solid phase transitions found.

Indeed, Figure 12 demonstrates the structural changes in the molecular packing of the five modifications of **1** occurring upon heating. As can be seen from the figure, there are the two different types of stacks in each of the modifications as well as two different types of their arrangement in the crystal structures. In the stable α_1 modification, the stacks are arranged in the chessboard order in such a way that stacks of one type run along the crystallographic axes perpendicular to them. Upon thermal expansion with an increase in temperature, most of the weak additional intermolecular interactions are broken. Then, the molecules of the β_1 modification twist and slightly rotate within the stacks in aspiration to form new additional intermolecular interactions. Furthermore, the stacks of one type move perpendicular to the *b*-axis and stay between the stacks of the second type, so the stacks of different types alternate along the *b*-axis. However, this structural readjustment results in three additional intermolecular interactions only. Obviously, this is the reason, why the β_1 modification of **1** is the least stable one and can readily undergo a phase transition into the β_2 modification. Remarkably, the molecular stacks in the β_2 modification closely resemble the stack arrangement in the α_1 modification. Moreover, the molecules within the stacks of one type twist even more as compared to the β_1 modification, while the molecules within the stacks of the second type keep the twist angle close to that in the β_1 modification. This crystal packing gives rise to 24 additional intermolecular interactions for the two crystallographically independent molecules (12 per molecule as average), and therefore, it is considerably more stable. Further, the packing of the stacks in the β_2 and β_3 modifications remains almost unchanged. However, the molecules of the β_2 modification characterized by the smaller twist angle undergo additional twisting, so the twist angles of all molecules in the β_3 modification get equal and close to that in the molecules of the β_2 modification characterized by the larger twist angle. Despite the total number of additional intermolecular interactions decreasing from 12 to 11 on going from the β_2 to β_3 modification, the additional twisting of molecules likely affords maximization of the intermolecular interactions upon unit cell volume expansion due to heating. A similar behavior was previously reported for β-phase of $Cu(pta)_2$ (pta = pivaloyltrifluoroacetonate) by Welsh and coworkers.[27] Moreover, all copper(II) atoms in the β_3 modification, contrary to the β_2 modification, adopt the energetically favorable [4 + 2] coordination geometry. Thus, (i) the single-crystal-to-single-crystal $\alpha_1 \rightleftharpoons \beta_1$ phase transition evidently requires only little energy expences, (ii) the suggested β_1-to-β_2 phase transition is, in fact, a reverse transition with respect to the $\alpha_1 \rightleftharpoons \beta_1$ one, (iii) the suggested β_2-to-β_3 phase transition should proceed with minimum structural rearrangement, and (iv) the β_1, β_2, and β_3 modifications should possess very similar unit cell volumes at any temperature. Consequently, as can be concluded from that said previously, the $\beta_1 \rightarrow \beta_2 \rightarrow \beta_3$ phase transitions should be energetically inexpensive and can really occur within the $\alpha_1 \rightarrow \gamma_1$ (as well as the $\beta_2 \rightarrow \beta_3$ phase transition really being able to occur within the $\beta_2 \rightarrow \gamma_1$ one) phase transition observed by DSC.

Finally, the $\beta_3 \rightarrow \gamma_1$ as well as $\alpha_1 \rightarrow \gamma_1$ and $\beta_2 \rightarrow \gamma_1$ phase transitions lead to some flattening and ordering of molecules within the stacks in such a manner that the high tetragonal symmetry is realized. These transformations can be explained by significant weakening of all intermolecular interactions in the γ_1 modification with the unit cell expansion upon heating. This explanation is confirmed by quantum-chemical simulations within the DFT framework for isolated molecules of **1** in all three phases α, β, and γ. Geometry optimization in all cases converged to the planar molecular structure actually observed for the γ phase. The vibration frequency calculations at the same level of theory demonstrated that exactly this molecular conformation corresponds to the global energy minimum in the gas phase. Evidently, the additional intermolecular interactions realized in the α_1, β_1, β_2, and β_3 modifications give rise to significant energy profit, which exceeds the differences between the global and local energy minima on the potential energy surface corresponding to the staircase-like and twisted conformations of **1**. Interestingly, even rapid unit cell volume contraction at low temperature in the γ_2 modification is not able to induce the change to the energetically favorable planar conformation quickly enough.

dx.doi.org/10.1021/ic300814w | *Inorg. Chem.* 2012, 51, 10590−10602

Table 6. Crystallographic Data for the α_1, β_1, β_2, β_3, γ_1, and γ_2 Modifications of 1

	α_1	β_1	β_2	β_3	γ_1	γ_2
empirical formula	$C_{10}H_4N_4F_{14}Cu$	$C_{10}H_4N_4F_{14}Cu$	$C_{10}H_4N_4F_{14}Cu$	$C_{10}H_4N_4F_{14}Cu$	$C_{10}H_4N_4F_{14}Cu$	$C_{10}H_4N_4F_{14}Cu$
fw	509.71	509.71	509.71	509.71	509.71	509.71
T, K	100(2)	363(2)	100(2)	300(2)	293(2)	100(2)
crystal size, mm^3	0.25 × 0.24 × 0.22	0.25 × 0.24 × 0.22	0.20 × 0.15 × 0.05	0.24 × 0.18 × 0.14	0.40 × 0.04 × 0.04	0.40 × 0.04 × 0.04
cryst syst	monoclinic	monoclinic	triclinic	monoclinic	tetragonal	tetragonal
space group	$P2_1/n$	$P2_1/c$	$P\bar{1}$	$P2_1/n$	$P4_2/n$	$P4_2/n$
a, Å	8.1027(5)	12.4673(19)	10.6799(15)	11.3475(12)	16.9722(7)	16.7731(3)
b, Å	9.7053(6)	10.1898(15)	12.1418(16)	12.8619(14)	16.9722(7)	16.7731(3)
c, Å	9.4485(6)	13.1267(19)	12.9618(19)	12.4521(13)	5.6208(5)	5.5775(2)
α, deg	90	90	86.992(3)	90	90	90
β, deg	90.608(1)	95.272(3)	89.995(3)	115.552(2)	90	90
γ, deg	90	90	67.385(2)	90	90	90
V, Å^3	742.98(8)	1660.6(4)	1549.1(4)	1639.6(3)	1619.1(2)	1569.16(7)
Z^a	2	4	4	4	4	4
d_c, g cm^{-3}	2.278	2.039	2.186	2.065	2.091	2.158
$F(000)$	494	988	988	988	988	988
μ, mm^{-1}	1.641	1.469	1.574	1.487	1.506	1.554
$2\theta_{max}$, deg	60.4	60.0	56.0	61.4	60.0	60.0
index range	$-11 \le h \le 11$	$-17 \le h \le 17$	$-14 \le h \le 14$	$-16 \le h \le 16$	$-23 \le h \le 23$	$-23 \le h \le 23$
	$-13 \le k \le 13$	$-14 \le k \le 14$	$-16 \le k \le 16$	$-18 \le k \le 18$	$-23 \le k \le 23$	$-23 \le k \le 23$
	$-13 \le l \le 13$	$-18 \le l \le 18$	$-17 \le l \le 17$	$-17 \le l \le 17$	$-7 \le l \le 7$	$-7 \le l \le 7$
no. rflns collected	9140	20 656	15 713	21 057	17 784	17 633
no. unique rflns	2169	4825	7367	5033	2341	2284
no. rflns with $I > 2\sigma(I)$	2046	2443	4853	3252	1438	1749
data/restraints/params	2169/0/133	4825/0/262	7367/0/523	5033/0/262	2341/0/133	2284/0/133
R1; wR2 ($I > 2\sigma(I)$)	0.021; 0.053	0.045; 0.107	0.051; 0.093	0.039; 0.103	0.039; 0.105	0.030; 0.070
R1; wR2 (all data)	0.023; 0.054	0.106; 0.126	0.118; 0.143	0.068; 0.120	0.069; 0.133	0.045; 0.084
GOF on F^2	1.000	1.003	1.003	1.002	1.001	1.002
T_{min}; T_{max}	0.684; 0.714	0.710; 0.738	0.744; 0.925	0.717; 0.819	0.584; 0.942	0.575; 0.940

[a]Z is defined as number of empirical formulas.

CONCLUSION

In summary, three thermochromic phases (α, green; β, red; γ, yellow) and six polymorphic modifications (α_1, β_1, β_2, β_3, γ_1, and γ_2) of copper(II) diiminate **1** have been found and structurally characterized. The α phase is thermodynamically stable at normal conditions, whereas the high-temperature β and γ phases can be quenched at room temperature in the metastable state, but they slowly transform into the stable α phase over several days or even weeks. The X-ray diffraction study revealed that the molecules of **1** in the α, β, and γ phases adopt different conformations, namely, staircase-like, twisted, and planar, respectively. The solid−solid phase transitions between the modifications of **1** ($\alpha_1 \rightleftharpoons \beta_1$, $\alpha_1 \rightarrow \gamma_1$, $\beta_2 \rightarrow \gamma_1$, $\beta_3 \rightarrow \gamma_1$, $\gamma_1 \rightleftharpoons \gamma_2$) triggered by temperature were studied using a combination of DSC, single-crystal X-ray diffraction, and quantum-chemical calculations. It has been suggested that, under equilibrium conditions, the $\alpha_1 \rightarrow \gamma_1$ and $\beta_2 \rightarrow \gamma_1$ phase transitions should proceed stepwise through the $\alpha_1 \rightarrow \beta_1 \rightarrow \beta_2 \rightarrow \beta_3 \rightarrow \gamma_1$ and $\beta_2 \rightarrow \beta_3 \rightarrow \gamma_1$ stages, respectively. The driving force of the solid−solid phase transitions is the rupture/reformation of additional weak intermolecular interactions upon heating/cooling.

Solid phase reversible thermochromism is an interesting and rather rare phenomenon in coordination chemistry.[28] Nevertheless, the thermochromic single-crystal-to-single-crystal green-red $\alpha_1 \rightleftharpoons \beta_1$ high-temperature phase transition is fully reversible at very low heating/cooling rates (smaller than 30 K/h) and can be repeated several times without significant degradation of the crystal quality.

Therefore, copper(II) diiminate **1** with this striking reversible interconversion can be considered as a new class of thermochromic materials. Solid state thermochromic behavior is of special interest for the design of devices for visual online monitoring of temperature changes. Crystalline materials exhibiting reversible temperature-induced phase transitions can be applied both as thermal sensors in calibration devices and as latent heat storage units capable of absorbing and releasing some amount of heat on demand. Smart phase change materials with fully reversible behavior without crystal quality degradation are an attractive target for scientists and a great challenge. Energy-saving materials from solar-cell systems are essential for environmentally friendly and sustainable development today.

EXPERIMENTAL SECTION

General Procedure. TGA was performed using a "Derivatograph-C" (MOM, Hungary) at a heating rate of 10 °C/min under an argon atmosphere. DSC measurements were carried out using a "DSC-822e" (Mettler-Toledo) at a heating/cooling rate of ±10 °C/min under an argon atmosphere. IR spectrum of solid **1** (KBr pellet, the stable α phase) was recorded on a Nicolet Magna IR-750 FTIR spectrometer in the range 300−3700 cm^{-1}. Mass-spectrum was measured on a mass-spectrometer Finnigan Polaris Q (electron ionization, 70 eV, ionic trap). UV−vis spectra of hexane solutions of green and red phases of **1** were obtained using a Carl Zeiss M-400 spectrophotometer. The elemental analysis was performed with a Carlo Erba EA1108 CHNS-O elemental analyzer.

*Copper Bis(1,1,1,3,5,5,5-heptafluoropentane-2,4-diiminate) (**1**).* A solution of 2-amino-4-iminoperfluoropent-2-ene (4.6 g) in $CHCl_3$

dx.doi.org/10.1021/ic300814w | Inorg. Chem. 2012, 51, 10590−10602

(20 mL) was added to a solution of $(CH_3COO)_2Cu$ (2.0 g) in distilled water (30 mL). The mixture was stirred for 30 min, and the organic layer was separated and washed with water. The solvent was then evaporated. The solid residue of 3.9 g (74.5%) was pure copper bis(1,1,1,3,5,5,5-heptafluoropentane-2,4-diiminate) in the form of dark green crystals. Mp = 167 °C. FT-IR (solid, ν/cm^{-1}): 324(w), 356(w), 406(w), 492(w), 532(m), 582(w), 634(m), 698(s), 738(m), 764(w), 822(w), 1018(m), 1144(s), 1182(s), 1218(s), 1246(s), 1324(s), 1386(m), 1436(m), 1476(s), 1558(m), 1612(m), 3366(w), 3370(s). UV−vis (hexane, λ_{max}/nm): 316, 364, 390. EIMS, m/z (%): 509 (58) $[M^+]$, 469 (42) $[C_{10}H_2F_{12}CuN_4]$, 441 (54) $[C_{10}H_2F_{12}CuN_2]$, 286 (78) $[C_5H_2F_7CuN_2]$, 235 (100) $[C_4HF_5CuN_2]$, 217 (58) $[C_4H_2F_4CuN_2]$, 225 (19) $[C_5H_4N_2F_7]$, 224 (19) $[C_5H_3N_2F_7]$, 155 (27) $[C_4H_3N_2F_4]$, 63 (36) $[Cu^+]$. Found (%): C 23.60; H 0.81; F 52.30; N 10.84. Calcd for $C_{10}H_4F_{14}CuN_4$ (M_r = 509.69) (%): C 23.56; H 0.79; F 52.18; N 10.99.

XANES Measurements. Cu K-edge X-ray absorption near-edge structure spectra for strictly single-phase green α_1 and red β_3 polymorphs of **1** as solids and their derived saturated benzene solutions have been measured at the "Structural Materials Science" beamline[29] of the Kurchatov Synchrotron Radiation Center (Moscow). The measurements for all samples have been performed in the transmission mode using two ionization chambers filled with appropriate N_2/Ar mixtures. The energy scale of the spectra has been calibrated by assigning a value of 8979 eV to the inflection point in the spectrum of Cu foil. The raw data reduction and linear-combination-fit analysis have been accomplished using the IFEFFIT software suite.[30]

X-ray Structure Determination. Data were collected using a Bruker APEX-II CCD diffractometer [λ(Mo K_α)-radiation, graphite monochromator, ω and φ scanning mode] and corrected for absorption using the *SADABS* program.[31] For details, see Table 6. The crystal structures of the α_1, β_1, β_2, β_3, γ_1, and γ_2 modifications of **1** were determined by direct methods and refined by a full-matrix least-squares technique on F^2 with anisotropic displacement parameters for non-hydrogen atoms. The hydrogen atoms were placed in calculated positions and refined within the riding model with fixed isotropic displacement parameters [U_{iso}(H) = 1.2U_{eq}(N)]. All calculations were carried out using the *SHELXTL* program.[32] Crystallographic data for the α_1, β_1, β_2, β_3, γ_1, and γ_2 modifications of **1** have been deposited with the Cambridge Crystallographic Data Center. CCDC 781589–781591, CCDC 837884, CCDC 837885, and CCDC 868939 contain supplementary crystallographic data for this paper. These data can be obtained free of charge from the Director, CCDC, 12 Union Road, Cambridge CB2 1EZ, U.K. (Fax: +44 1223 336033. E-mail: deposit@ccdc.cam.ac.uk or www.ccdc.cam.ac.uk.)

Quantum-Chemical Calculations. All computations of the crystal structures of **1** were carried out using the VASP 5.2.12 code.[33−36] Conjugated gradient technique was used for the optimization of atomic positions (started from experimental data), cell vectors, and minimization of the total energy. Projected augmented wave (PAW) method was applied to account for core electrons, while valence electrons were approximated by plane-wave expansion with a cutoff at 544 eV. Exchange and correlation terms of total energy were described by the PBE exchange-correlation functional. Kohn−Sham equations were integrated using the Γ-point approximation. To account for errors due to a poor description of van der Waals interactions by pure DFT functionals, the dispersion correction in terms of the Grimme's scheme was applied.[37] At the final step of our calculations, the convergence of atomic displacements was better than 0.01 eV $Å^{-1}$, and the energy variations were below 10^{-4} eV. To perform the topological analysis, the electron density distribution function was calculated on a dense FFT (fast Fourier transformation) grid (stepsize <0.03 Å) using PAWs with smallest core radii (the so-called "hard PAWs"). The topological analysis was carried out by the AIM program (a part of the ABINIT software suite).[38]

The DFT geometry optimization for isolated molecules of all three α, β, and γ phases was performed with the Gaussian 03 software package[39] at the M05-2x level of theory using 6-311G** basis set, starting from experimental X-ray molecular structures. The common convergence criteria of 3.0×10^{-4}, 4.5×10^{-4}, 1.2×10^{-3}, and 1.8×10^{-3} were applied to the gradients of the root mean square (rms) force, maximum force, rms displacement, and maximum displacement vectors, respectively.

■ ASSOCIATED CONTENT

Ⓢ Supporting Information

Full crystallographic data as CIF files and X-ray powder patterns of the green α_1 and red β_3 modifications of **1** along with indexing listings. This material is available free of charge via the Internet at http://pubs.acs.org.

■ AUTHOR INFORMATION

Corresponding Author

*E-mail: vkh@xray.ineos.ac.ru. Phone: +7 (499) 135 9343. Fax: +7 (499) 135 5085.

Notes

The authors declare no competing financial interest.

■ ACKNOWLEDGMENTS

We thank I.V. Ananyev for the help in quantum-chemical calculations and the Russian Foundation for Basic Research (Grants 11-03-00652 and 10-03-00505) for financial support of this work.

■ REFERENCES

(1) Bernstein, J. *Polymorphism in Molecular Crystals*; IUCr Monographs on Crystallography 14; Clarendon Press: Oxford, U.K., 2002.

(2) (a) Gafner, G.; Herbstein, F. H. *Acta Crystallogr.* **1960**, *13*, 706–716. (b) Gafner, G.; Herbstein, F. H. *Acta Crystallogr.* **1964**, *17*, 982–985.

(3) Fernandes, M. A.; Levendis, D. C.; Schoening, F. R. *Acta Crystallogr.* **2004**, *B60*, 300–314.

(4) Kaftory, M.; Botoshansky, M.; Kapon, M.; Shteiman, V. *Acta Crystallogr.* **2001**, *B57*, 791–799.

(5) Boese, R.; Polk, M.; Blaser, D. *Angew. Chem., Int. Ed. Engl.* **1987**, *26*, 245–247.

(6) Fabbiani, F. P. A.; Allan, D. R.; Parsons, S.; Pulham, C. R. *CrystEngComm* **2005**, *7*, 179–186.

(7) Herbstein, F. H. *Acta Crystallogr.* **2006**, *B62*, 341–383 and references therein.

(8) Dunitz, J. D.; Bernstein, J. *Acc. Chem. Res.* **1995**, *28*, 193–200.

(9) (a) Ma, J. P.; Dong, Y.-B.; Huang, R.-Q.; Smith, M. D.; Su, C.-Y. *Inorg. Chem.* **2005**, *44*, 6143–6145. (b) Zhang, Y.-J.; Liu, T.; Kanegawa, S.; Sato, O. *J. Am. Chem. Soc.* **2009**, *131*, 7942–7943.

(10) (a) Willett, R. D.; Ferraro, J. R.; Choca, M. *Inorg. Chem.* **1974**, *13*, 2919–2921. (b) Grenthe, I.; Paoletti, P.; Sandstroem, M.; Glikberg, S. *Inorg. Chem.* **1979**, *18*, 2687–2692. (c) Bloomquist, D. R.; Willett, R. D. *Coord. Chem. Rev.* **1982**, *47*, 125–164.

(11) Said-Galiyev, E.; Nikitin, L.; Vinokur, R.; Gallyamov, M.; Kurykin, M.; Petrova, O.; Lokshin, B.; Volkov, I.; Khokhlov, A.; Schaumburg, K. *Ind. Eng. Chem. Res.* **2000**, *39*, 4891–4896.

(12) Filyakova, T. I.; Saloutina, L. V.; Slepukhin, P. A.; Saloutin, V. I.; Chupakhin, O. N. *Russ. Chem. Bull.* **2009**, *58*, 1132–1138.

(13) (a) Polyanskaya, T. M.; Rozhdestvenskaya, I. V.; Martynova, T. N. *J. Struct. Chem.* **1992**, *34*, 420. (b) Toscano, P. J.; Dettelbacher, C.; Waechter, J.; Pavri, N. P.; Hunt, D. H.; Eisenbraun, E. T.; Zheng, B.; Kaloyeros, A. E. *J. Coord. Chem.* **1996**, *38*, 319. (c) Maverick, A. W.; Fronczek, F. R.; Maverick, E. F.; Billodeaux, D. R.; Cygan, Z. T.; Isovitsch, R. A. *Inorg. Chem.* **2002**, *41*, 6488–6499. (d) Higashiya, S.; Banger, K. K.; Ngo, S. C.; Lim, P. N.; Toscano, P. J.; Welch, J. T. *Inorg. Chim. Acta* **2003**, *351*, 291–304. (e) Baidina, I. A.; Krisyuk, V. V.; Stabnikov, P. A. *Russ. J. Struct. Chem.* **2006**, *47*, 1111–1116.

(14) Bader, R. W. F. *Atoms in Molecules: A Quantum Theory*; Oxford University Press: New York, 1990.

(15) Espinosa, E.; Molins, E.; Lecomte, C. *Chem. Phys. Lett.* **1998**, *285*, 170−173.
(16) Kitaigorodskii, A. I. General view on molecular packing. In *Advances in Structure Research by Diffraction Methods*; Brill, R., Mason, R., Eds.; Pergamon Press: Oxford, U.K., 1970, Vol. 3, pp 173−247.
(17) Penner-Hahn, J. E. X-Ray absorption spectroscopy. In *Comprehensive Coordination Chemistry II*; McCleverty, J. A., Meyer, T. J., Eds.; Elsevier: Oxford, U.K., 2004; pp 159−186.
(18) (a) Friscic, T.; MacGillivray, L. R. Z. *Kristallografiya* **2005**, *220*, 351−363. (b) Garcia-Garibay, M. A. *Angew. Chem., Int. Ed.* **2007**, *46*, 8945−8947. (c) MacGillivray, L. R.; Papaefstathiou, G. S.; Friscic, T.; Hamilton, T. D.; Bucar, D.-K.; Chu, Q.; Varshney, D. B.; Georgiev, I. G. *Acc. Chem. Res.* **2008**, *41*, 280−291. (d) Lauher, J. W.; Fowler, F. W.; Goroff, N. S. *Acc. Chem. Res.* **2008**, *41*, 1215−1229.
(19) Halder, G. J.; Kepert, C. J. *Aust. J. Chem.* **2006**, *59*, 597−604.
(20) (a) Evers, J.; Klapotke, T. M.; Mayer, P.; Oehlinger, G.; Welch, J. *Inorg. Chem.* **2006**, *45*, 4996−5007. (b) For a nonreversible phase transition between discrete complexes, see: Mobin, S. M.; Srivastava, A. K.; Mathur, P.; Lahiri, G. K. *Inorg. Chem.* **2009**, *48*, 4652−4654.
(21) (a) Lever, A. B. P.; Mantovani, E. *Inorg. Chem.* **1971**, *10*, 817−826. (b) Lever, A. B. P.; Mantovani, E.; Donini, J. C. *Inorg. Chem.* **1971**, *10*, 2424−2427.
(22) Kennedy, B. P.; Lever, A. B. P. *J. Am. Chem. Soc.* **1973**, *95*, 6907−6913.
(23) Fabbrizzi, L.; Micheloni, M.; Paoletti, P. *Inorg. Chem.* **1974**, *13*, 3019−3021.
(24) (a) Ferraro, J. R.; Basile, L. J.; Garcia-Ineguez, L. R.; Paoletti, P.; Fabbrizzi, L. *Inorg. Chem.* **1976**, *15*, 2342−2345. (b) Ferraro, J. R.; Fabbrizzi, L.; Paoletti, P. *Inorg. Chem.* **1977**, *16*, 2127−2129.
(25) Grenthe, I.; Paoletti, P.; Sandstroem, M.; Glikberg, S. *Inorg. Chem.* **1979**, *18*, 2687−2692.
(26) Riley, M. J.; Neill, D.; Bernhardt, P. V.; Byriel, K. A.; Kennard, C. H. L. *Inorg. Chem.* **1998**, *37*, 3635−3639.
(27) DelaRosa, M. J.; Banger, K. K.; Higashiya, S.; Ngo, S. C.; Hunt, D. H.; Bousman, K. S.; Toscano, P. J.; Welsh, J. T. *J. Fluor. Chem.* **2003**, *123*, 109−117.
(28) Sone, K.; Fukuda, Y. *Inorganic Thermochromism*; Springer-Verlag: Heidelberg, 1987.
(29) Chernyshov, A. A.; Veligzhanin, A. A.; Zubavichus, Y. V. *Nucl. Instrum. Methods Phys. Res., Sect. A* **2009**, *603*, 95−98.
(30) Ravel, B.; Newville, M. *J. Synchrotron Radiat.* **2005**, *12*, 537−541.
(31) Sheldrick, G. M. *SADABS, v. 2.03, Bruker/Siemens Area Detector Absorption Correction Program*; Bruker AXS: Madison, WI, 2003.
(32) Sheldrick, G. M. *Acta Crystallogr.* **2008**, *A64*, 112−122.
(33) Kresse, G.; Hafner, J. *Phys. Rev.* **1993**, *B47*, 558−561.
(34) Kresse, G.; Furthmuller, J. *Comput. Mater. Sci.* **1996**, *6*, 15−50.
(35) Kresse, G. Thesis. Technische Universitat, Wien, 1993.
(36) Kresse, G.; Furthmuller, J. *Phys. Rev.* **1996**, *B54*, 11169−11186.
(37) Grimme, S. *J. Comput. Chem.* **2006**, *27*, 1787−1799.
(38) Gonze, X.; Beuken, J.-M.; Caracas, R.; Detraux, F.; Fuchs, M.; Rignanese, G.-M.; Sindic, L.; Verstraete, M.; Zerah, G.; Jollet, F.; Torrent, M.; Roy, A.; Mikami, M.; Ghosez, P.; Raty, J.-Y.; Allan, D. C. *Comput. Mater. Sci.* **2002**, *25*, 478−492.
(39) Frisch, M. J.; Trucks, G. W.; Schlegel, H. B.; Scuseria, G. E.; Robb, M. A.; Cheeseman, J. R.; Montgomery, J. A., Jr.; Vreven, T.; Kudin, K. N.; Burant, J. C.; Millam, J. M.; Iyengar, S. S.; Tomasi, J.; Barone, V.; Mennucci, B.; Cossi, M.; Scalmani, G.; Rega, N.; Petersson, G. A.; Nakatsuji, H.; Hada, M.; Ehara, M.; Toyota, K.; Fukuda, R.; Hasegawa, J.; Ishida, M.; Nakajima, T.; Honda, Y.; Kitao, O.; Nakai, H.; Klene, M.; Li, X.; Knox, J. E.; Hratchian, H. P.; Cross, J. B.; Adamo, C.; Jaramillo, J.; Gomperts, R.; Stratmann, R. E.; Yazyev, O.; Austin, A. J.; Cammi, R.; Pomelli, C.; Ochterski, J. W.; Ayala, P. Y.; Morokuma, K.; Voth, G. A.; Salvador, P.; Dannenberg, J. J.; Zakrzewski, V. G.; Dapprich, S.; Daniels, A. D.; Strain, M. C.; Farkas, O.; Malick, D. K.; Rabuck, A. D.; Raghavachari, K.; Foresman, J. B.; Ortiz, J. V.; Cui, Q.; Baboul, A. G.; Clifford, S.; Cioslowski, J.; Stefanov, B. B.; Liu, G.; Liashenko, A.; Piskorz, P.; Komaromi, I.; Martin, R. L.; Fox, D. J.; Keith, T.; Al-Laham, M. A.; Peng, C. Y.; Nanayakkara, A.; Challacombe, M.; Gill, P. M. W.; Johnson, B.; Chen, W.; Wong, M. W.; Gonzalez, C. Pople, J. A. *Gaussian 03 (Revision B.05)*; Gaussian, Inc.: Pittsburgh, PA, 2003.